Copy No. _____

Defence Research and Development Canada
Recherche et développement pour la défense Canada

DEFENCE R&D DÉFENSE

Effects of composition on the properties of magnetic shape memory alloys

R.A. Dunlap
Weathervane Scientific Incorporated

Weathervane Scientific Incorporated
P.O. Box 31030
Halifax, Nova Scotia
B3K 5T9

Project Manager: Dr. Richard A. Dunlap, 902-889-3535
Contract Number: W7707-042846/001/HAL
Contract Scientific Authority: Dr. Shannon P. Farrell, 902-427-3437

Defence R&D Canada – Atlantic

Contract Report
DRDC Atlantic CR 2006-042
March 2007

Canada

This page intentionally left blank.

Effects of composition on the properties of magnetic shape memory alloys

R.A. Dunlap
Weathervane Scientific Incorporated

Weathervane Scientific Incorporated
P.O. Box 31030
Halifax, Nova Scotia
B3K 5T9

Project Manager: Dr. Richard A. Dunlap, 902-889-3535

Contract number: W7707-042846/001/HAL

Contract Scientific Authority: Dr. Shannon P. Farrell, 902-427-3437

Defence R&D Canada – Atlantic

Contract Report

DRDC Atlantic CR 2006-042

March 2007

Author

Original signed by Dr. Richard A. Dunlap

Dr. Richard A. Dunlap

Approved by

Original signed by Dr. Shannon P. Farrell

Dr. Shannon P. Farrell

Contract Scientific Authority

Approved for release by

Original signed by Jim L. Kennedy

Kirk Foster

DRP Chair

Terms of Release:

The Scientific or technical validity of this Contract Report is entirely the responsibility of the contractor and the contents do not necessarily have the approval or endorsement of Defence R&D Canada.

Abstract

Magnetic shape memory alloys based on the Heusler alloy Ni_2MnGa have been investigated experimentally and the magnetic interactions have been modeled on the basis of the indirect exchange coupling of localized magnetic moments. A variety of techniques including x-ray diffraction, differential scanning calorimetry, thermogravimetric analysis, magnetization and Mössbauer effect spectroscopy have been utilized to measure the structural, thermal and magnetic properties of these alloys. Analysis of these results suggests that alloys containing a few at% Fe may be the most suitable for further exploration as commercially viable magnetic shape memory alloys. Theoretical investigations have shown that the indirect exchange coupling of magnetic moments associated with Mn ions on the Mn sites with other Mn-site Mn moments is ferromagnetic. This is also the case for Ni site moments associated with Ni ions. The coupling between Mn-site Mn moments and Mn ions located on Ni or Ga sites is antiferromagnetic. These observations explain the composition dependence of the saturation magnetization and the Curie temperature in off-stoichiometric Ni_2MnGa alloys.

Résumé

Nous avons étudié les alliages à mémoire de forme magnétiques (MFM) basés sur l'alliage Heusler Ni_2MnGa, et modélisé leurs interactions magnétiques sur la base du couplage d'échange indirect des moments magnétiques localisés. Nous avons utilisé diverses techniques — notamment la diffraction des rayons X, l'analyse calorimétrique à compensation de puissance, l'analyse thermogravimétrique, la magnétisation et la spectroscopie Mössbauer — pour mesurer les propriétés structurales, thermiques et magnétiques de ces alliages. L'analyse des résultats porte à croire que les alliages ne contenant que quelques pourcents de Fe seraient pour lesquels des travaux supplémentaires visant à leur donner une viabilité commerciale seraient les plus susceptibles de porter fruit. Les études théoriques démontrent que le couplage d'échange indirect des moments magnétiques des ions Mn sur les sites de Mn avec d'autres moments des ions Mn sur des sites Mn est du type ferromagnétique. C'est également le cas des moments des sites de Ni associés aux ions Ni. Le couplage entre les moments des ions Mn sur les sites Mn et ceux des ions Mn localisés sur des sites de Ni ou de Ga est du type antiferromagnétique. Ces observations expliquent la dépendance de la magnétisation de saturation et du point de Curie par rapport de la composition dans les alliages Ni_2MnGa non stœchiométriques.

This page intentionally left blank.

Executive summary

Introduction: The Emerging Materials Section of Defence R&D Canada - Atlantic has been developing magnetic shape memory alloys (MSMA) for use in a variety of defence applications (sensors, actuators and energy harvesting devices). MSM materials are a class of smart materials that change shape in response to application of a magnetic field or compressive strain through the reorientation of twin variants. The Heusler alloy Ni_2MnGa (near stoichiometry) is probably the most widely studied material in this class. The application of this material relies upon the engineering of materials with appropriate physical properties.

One method of controlling alloy properties is by the preparation of off-stoichiometric alloys or alloys with atomic substitutions. An understanding of how alloy composition affects the relevant physical properties is important for the efficient design of useful materials. In the present work we have undertaken both experimental and theoretical studies of Ni-Mn-Ga based alloys in order to better understand the composition dependence of their magnetic properties.

Significance: This study is part of an effort for the development of magnetically active materials for use as sensor/actuator and energy harvesting materials for use by the Canadian Forces. The use of various techniques for investigation, characterization and overall assessment of properties has narrowed in on a range of compositions that shows promise for development of new MSMA. The theoretical studies have provided a firm basis for understanding the magnetic interactions in these materials.

Results: The experimental results obtained here have provided information about the magnetic properties of Ni-Mn-Ga based alloys. Substitution of a small amount of Fe has shown the most promising magnetic and structural properties in terms of structural transition temperatures, Curie temperatures and magnetization. Theoretical studies have helped clarify the fundamental interactions that are responsible for the magnetic behaviour.

Future plans: Further studies include combinatorial materials science methods to produce a wide range of compositions of Ni-Mn-Ga-Fe and, eventually, growth and investigation of oriented single crystals. A combination of characterization and theoretical modeling of Fe-containing alloys will clarify the relationship of the Fe magnetic moment to the overall properties of the alloy.

Dunlap, R.A. 2007. Effects of composition on the properties of magnetic shape memory alloys. DRDC Atlantic CR 2006-042. Defence R&D Canada - Atlantic.

Sommaire

Introduction : La Section des nouveaux matériaux de R et D pour la défense Canada – Atlantique met au point des alliages à mémoire de forme magnétiques (MFM) qui seront employés dans diverses applications militaires (senseurs, actionneurs et dispositifs de captage d'énergie). Les matériaux MFM sont une classe de matériaux intelligents qui changent de forme en réponse à l'application d'un champ magnétique ou d'une déformation de compression par la réorientation des variantes jumelles. L'alliage Heusler Ni_2MnGa (quasi stœchiométrique) est probablement le matériau le plus étudié dans cette classe. L'application de ces matériaux est tributaire de leur conception technique, et ils doivent présenter les propriétés physiques appropriées.

Une façon de contrôler les propriétés d'un alliage consiste à préparer des alliages non stœchiométriques ou des alliages avec substitutions atomiques. Pour concevoir efficacement des matériaux utiles, il importe de comprendre comment la composition des alliages affecte les propriétés physiques pertinentes. Dans le cadre de ce travail, nous avons entrepris l'étude expérimentale et théorique des alliages à base de Ni-Mn-Ga, afin de mieux comprendre la dépendance de leurs propriétés magnétiques à l'égard de leur composition.

Portée : Cette étude fait partie d'un programme visant à développer des matériaux magnétiquement actifs, susceptibles d'être utilisés par les Forces canadiennes dans des capteurs, des actionneurs et des matériaux de récolte d'énergie. L'utilisation de diverses techniques d'analyse, la caractérisation des matériaux et l'évaluation globale des propriétés nous ont permis de restreindre la plage de composition aux matériaux qui semblent prometteurs pour le développement des nouveaux AMFM. Les études théoriques nous ont permis de bien comprendre les interactions magnétiques de ces matériaux.

Résultats : Les résultats théoriques obtenus dans le cadre de ces travaux nous ont fourni des données sur les propriétés magnétiques des alliages à base de Ni-Mn-Ga. La substitution de faibles quantités de Fe a donné un matériau qui présente les propriétés magnétiques et structurales les plus prometteuses en termes de températures de transition structurale, de point de Curie et de magnétisation. Les études théoriques nous ont également aidé à clarifier les interactions fondamentales qui sont responsables du comportement magnétique.

Recherches futures : Dans le cadre de nos recherches futures, nous utiliserons les méthodes combinatoires des sciences des matériaux afin de produire un large éventail de composition d'alliages de type Ni-Mn-Ga-Fe et, en définitive, nous fabriquerons et étudierons des monocristaux orientés. Une combinaison de travaux de caractérisation et de modélisation théorique des alliages contenant du Fe nous permettra de clarifier la relation entre le moment magnétique du Fe et les propriétés globales de l'alliage.

Dunlap, R.A. 2007. Effects of composition on the properties of magnetic shape memory alloys (*Effets de la composition des alliages à mémoire de forme magnétique sur leurs propriétés*). RDDC Atlantique CR 2006-042. R et D pour la défense Canada – Atlantique.

Table of contents

List of figures

List of tables

Acknowledgements

The author is grateful to J. Chen, E. Dunlap, G. Fisher, D.J.W. Geldart, I. Keough, J.D. McGraw and M. Stancescu for their contributions to this work.

1. Introduction

The Heusler alloy Ni_2MnGa has attracted much attention as a magnetic shape memory alloy due to the presence of a martensitic transition in the ferromagnetic regime. The application of this and similar materials as (e.g.) sensors or actuators, relies upon the engineering of materials with appropriate physical properties such as, martensitic transition temperature, Curie temperature, saturation magnetization and magnetic anisotropy energy. One method of controlling alloy properties is by the preparation of off-stoichiometric alloys or alloys with atomic substitutions. An understanding of how alloy composition affects the relevant physical properties is important for the efficient design of useful materials. In recent years there have been a number of studies of the effects of composition on magnetic properties and much is known from an empirical standpoint. Specifically the effects of stoichiometry in Ni-Mn-Ga [1-2] as well as the influence of substitutional atoms [3-5] have been reported. Also of relevance, is the investigation of the pressure dependence of the magnetic properties of these materials [6].

It is known that the overall strength of the magnetic interactions in Ni-Mn-Ga is a maximum (as evidenced by the Curie temperature) for the Heusler stoichiometry, Ni_2MnGa. It is also known that alloys with either more Mn or with less Mn have lower Curie temperatures. That is, for alloys of the form $Ni_xMn_yGa_z$ ($x+y+z = 100$) the Curie temperature is a maximum for $y = 25$ (the $L2_1$ Heusler stoichiometry). The reduction in Curie temperature for alloys with $y < 25$ may be a direct consequence of the dilution of the magnetic moment carrying Mn ions. For alloys with $y > 25$, Enkovaara et al. [7] have suggested that the magnetic properties are the result of antiferromagnetic coupling of the excess Mn ions. For alloys with substitutions, changes in the Curie temperature have been correlated to changes in the lattice parameter that result from the ionic radius of the substitutional atoms [3,4].

In the present contract the properties of Ni-Mn-Ga based magnetic shape memory alloys have been investigated both from an experimental and a theoretical approach. Alloys with different stoichiometries as well as different elemental additions have been studied. Experimental measurements of structural and magnetic properties have been performed in order to better understand the systematics of the behavior of these materials. Theoretical modeling of the magnetic interactions in these materials has been undertaken in order to understand the radial dependence of the indirect exchange interaction as well as the relationship of bulk magnetic properties to the underlying crystal structure and composition. More detailed experimental measurements have been made on three selected alloys that form a basis for the systematic comparison of theoretical and experimental results.

2. Experimental Approach

2.1 Experimental Methods

Alloys of the compositions as given in Table 1 have being prepared. Alloys were arc melted followed by etching for two hours in a solution of 2% HNO_3 in methanol. Ingots were ground and the powders were annealed in quartz ampoules under argon. Annealing was performed at 800 °C for 3 days followed by cooling to 500 °C, annealing for 1 day and slow cooling.

Table 1: *Composition of samples.*

sample	**composition**
D1	$Ni_{49.5}Mn_{28.3}Ga_{21}Fe_{1.2}$
D2	$Ni_{49}Mn_{26}Ga_{21}Fe_{4}$
D3	$Ni_{49}Mn_{20}Ga_{23}Fe_{8}$
D4	$Ni_{53}Mn_{23}Ga_{23}Fe_{1}$
D5	$Ni_{52}Mn_{20}Ga_{24}Fe_{4}$
D6	$Ni_{52}Mn_{16}Ga_{24}Fe_{8}$
D7	$Ni_{54}Mn_{20}Ga_{25}Fe_{1}$
D8	$Ni_{49}Mn_{28}Ga_{22}Cu_{1}$
D9	$Ni_{49}Mn_{28}Ga_{22}Co_{1}$
D10	$Ni_{49.5}Mn_{28}Ga_{21.5}V_{1}$
D11	$Ni_{49.5}Mn_{28}Ga_{21.5}Cr_{1}$
D14	$Ni_{49.5}Mn_{28.3}Ga_{21.2}Sb_{1}$
D15	$Ni_{49.5}Mn_{28.3}Ga_{21.2}Sn_{1}$
D16	$Ni_{49.5}Mn_{28.3}Ga_{21.2}In_{1}$
D17	$Ni_{49.5}Mn_{28.3}Ga_{21.2}Si_{1}$
D18	$Ni_{49.5}Mn_{28.3}Ga_{21.2}Ge_{1}$
D19	$Ni_{49.5}Mn_{28.9}Ga_{21.5}B_{0.1}$
D20	$Ni_{54}Mn_{20.9}Ga_{25}B_{0.1}$
D21	$Ni_{50}Mn_{25}Ga_{21}Fe_{4}$
D22	$Ni_{50}Mn_{21}Ga_{25}Fe_{4}$
A14	$Ni_{47.5}Mn_{32}Ga_{18}Ti_{2.5}$

Room temperature X-ray diffraction (XRD) scans were made on all annealed samples using a Philips X'Pert scanning diffractometer with Cu-K_α radiation for scattering angles (2θ) from 20 to 100 degrees.

Differential scanning calorimetry (DSC) measurements of annealed samples were made over a temperature range of about - 80 °C to 200 °C on a TA Instruments Q1000 DSC. These measurements used samples in the range of 5 - 15 mg. Measurements were made during both heating and cooling.

Thermogravimetric analysis (TGA) was performed on all annealed samples over a temperature range of about 20 °C to 150 °C on a TA Instruments Q500 TGA. Measurements used samples of approximately 10 mg. Curie temperatures were determined from the TGA scans as described in reference [8]. Measurements were made during heating.

Vibrating sample magnetometry (VSM) measurements were made on all samples at room temperature and in applied fields up to 0.8 T using a PAR-155 VSM. The magnetic field was measured using a calibrated Hall probe and the magnetization was calibrated to the room temperature magnetization of a high purity Ni standard (54.4 emu/g). Typical sample masses were 50 -130 mg.

Magnetic properties of selected samples have also been measured using the Physical Properties Measurement System (PPMS) available through the Institute for Research on Materials, Dalhousie University. Hysteresis loops at room temperature and at 20 K were obtained in applied fields of up to 4 T.

A room temperature ^{57}Fe Mössbauer effect spectrum has been obtained for one of the Fe-containing samples (D3) using a $\underline{Rh}^{57}Co$ source and a Wissel System II spectrometer operating in the constant acceleration mode. The spectrum has been referenced to room temperature α-Fe.

2.2 Experimental Results

Results of x-ray measurements are summarized in Table 2. A typical x-ray diffraction scan of a cubic phase ($L2_1$) sample (D2) is illustrated in Figure 1 along with the identification of the peak indices. The table gives the observed room temperature phase along with the measured lattice parameter for the cubic phase alloys.

A typical DSC scan of a sample with austenite and martensite transitions above room temperature (D1) is shown in Figure 2. The peaks on heating and cooling near 50 °C are from the austenite and martensite transitions, respectively, and start (A_S and M_S) and finish (A_F and M_F) transition temperatures obtained from these measurements are summarized in Table 3. The small peaks near 100 °C correspond to the Curie transition. The Curie transition does not show clear, well-defined features in all DSC scans and is better observed from TGA scans. A TGA scan (for D8) is shown in Figure 3. The Curie temperature as obtained from the TGA measurements as well as values obtained during heating and cooling from DSC measurements (where possible), are given in Table 4.

Table 2: *Sample compositions and x-ray diffraction results.*

sample	composition	structure	a (Å)
D1	$Ni_{49.5}Mn_{28.3}Ga_{21}Fe_{1.2}$	orthorhombic	-
D2	$Ni_{49}Mn_{26}Ga_{21}Fe_{4}$	cubic	5.8093
D3	$Ni_{49}Mn_{20}Ga_{23}Fe_{8}$	cubic	5.8065
D4	$Ni_{53}Mn_{23}Ga_{23}Fe_{1}$	orthorhombic	-
D5	$Ni_{52}Mn_{20}Ga_{24}Fe_{4}$	cubic	5.7971
D6	$Ni_{52}Mn_{16}Ga_{24}Fe_{8}$	cubic	5.7869
D7	$Ni_{54}Mn_{20}Ga_{25}Fe_{1}$	orthorhombic	-
D8	$Ni_{49}Mn_{28}Ga_{22}Cu_{1}$	cubic	5.827
D9	$Ni_{49}Mn_{28}Ga_{22}Co_{1}$	cubic	5.8357
D10	$Ni_{49.5}Mn_{28}Ga_{21.5}V_{1}$	cubic	5.8372
D11	$Ni_{49.5}Mn_{28}Ga_{21.5}Cr_{1}$	cubic	5.8457
D14	$Ni_{49.5}Mn_{28.3}Ga_{21.2}Sb_{1}$	cubic	5.8313
D15	$Ni_{49.5}Mn_{28.3}Ga_{21.2}Sn_{1}$	cubic	5.8366
D16	$Ni_{49.5}Mn_{28.3}Ga_{21.2}In_{1}$	uncertain	-
D17	$Ni_{49.5}Mn_{28.3}Ga_{21.2}Si_{1}$	cubic	5.8277
D18	$Ni_{49.5}Mn_{28.3}Ga_{21.2}Ge_{1}$	cubic?	5.8478
D19	$Ni_{49.5}Mn_{28.9}Ga_{21.5}B_{0.1}$	cubic?	5.8413
D20	$Ni_{54}Mn_{20.9}Ga_{25}B_{0.1}$	cubic	5.802
D21	$Ni_{50}Mn_{25}Ga_{21}Fe_{4}$	orthorhombic	-
D22	$Ni_{50}Mn_{21}Ga_{25}Fe_{4}$	cubic	5.8205
A14	$Ni_{47.5}Mn_{32}Ga_{18}Ti_{2.5}$	cubic	5.8263

Notes: lattice parameters are calculated for cubic austenite samples

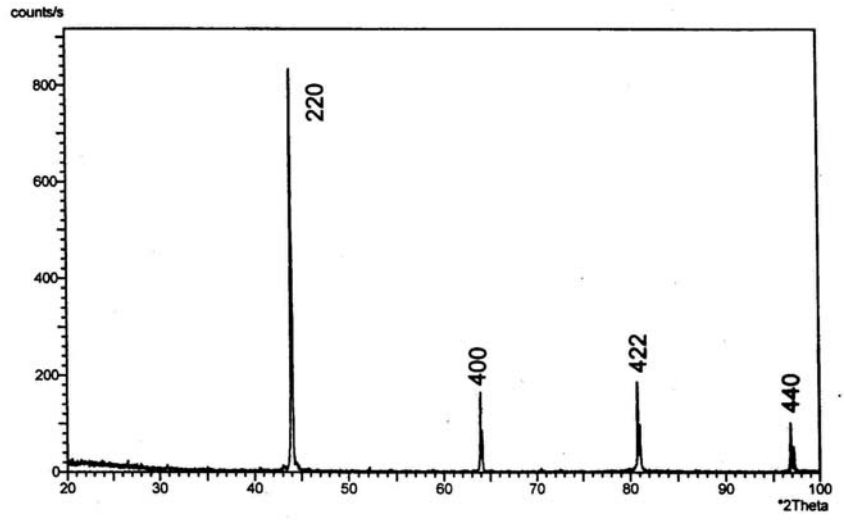

Figure 1: *Room temperature Cu-Ka x-ray diffraction pattern of sample D2. Miller indices of the cubic $L2_1$ phase are indicated. Results are summarized in Table 2.*

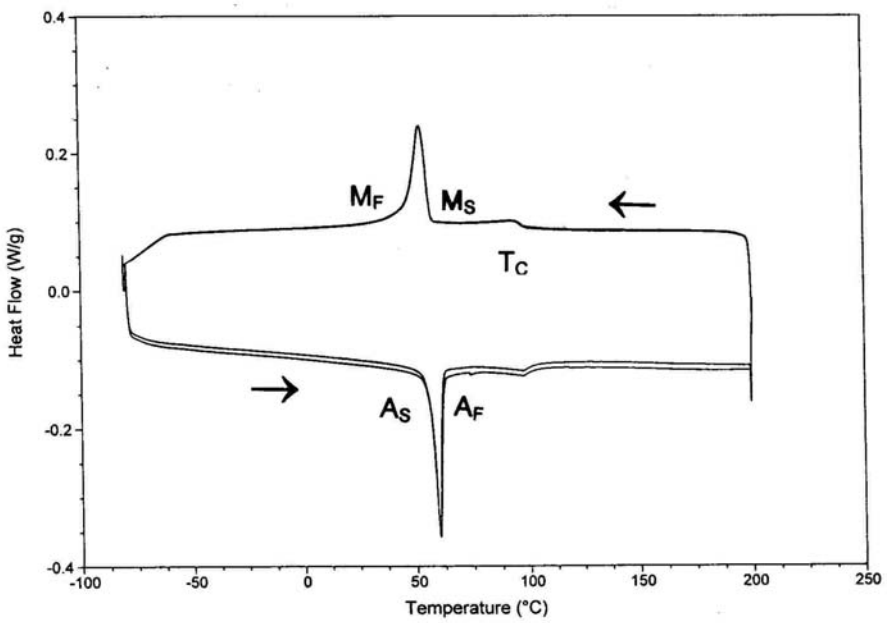

Figure 2: *DSC scan of sample D1. The arrows indicate the direction of heating and cooling. Austenite start and finish temperatures, A_S and A_F (on heating) and martensite start and finish temperatures, M_S and M_F (on cooling) are indicated in the figure and are summarized in Table 3.*

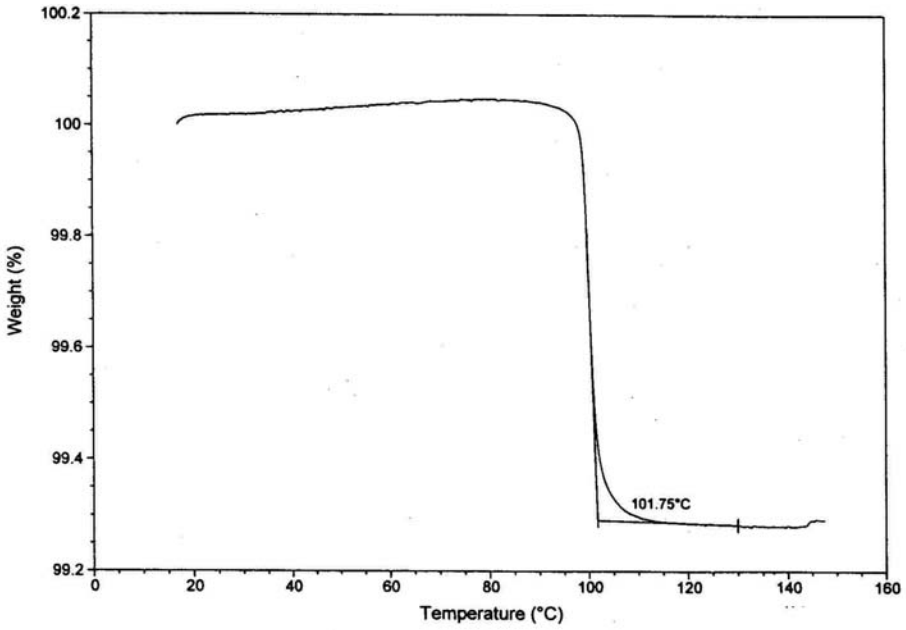

Figure 3: *TGA scan of sample D8. The Curie temperature is observed as the temperature at which the weight extrapolates to the background value. The value is indicated in Table 4.*

Room temperature hysteresis loops obtained from vibrating sample magnetometry are illustrated in Figure 4. In general the samples that show a cubic structure at room temperature are well saturated in an external field of 0.8 T. Those that show a non-cubic structure are generally not fully saturated at 0.8 T. Those that have a non-cubic structure possess a hard magnetic axis and in a random powdered sample this contributes to the high field susceptibility. Magnetization measured in an applied field of 0.8 T is summarized in Table 4. For the cubic samples, this can be assumed to be close to the full room temperature saturation magnetization while for the non-cubic samples the actual saturation magnetization is likely to be slightly larger than the value in the table. This is discussed further with regard to the PPMS measurements.

***Table 3**: Observed transition temperatures from DSC measurements.*

sample	composition	A_S (°C)	A_F (°C)	M_S (°C)	M_F (°C)
D1	$Ni_{49.5}Mn_{28.3}Ga_{21}Fe_{1.2}$	55	62	57	46
D2	$Ni_{49}Mn_{26}Ga_{21}Fe_4$	15	33	17	6
D3	$Ni_{49}Mn_{20}Ga_{23}Fe_8$	-	-	-	-
D4	$Ni_{53}Mn_{23}Ga_{23}Fe_1$	56	84	76	43
D5	$Ni_{52}Mn_{20}Ga_{24}Fe_4$	-	-	-	-
D6	$Ni_{52}Mn_{16}Ga_{24}Fe_8$	-39	-15	-38	-60
D7	$Ni_{54}Mn_{20}Ga_{25}Fe_1$	24	48	33	9
D8	$Ni_{49}Mn_{28}Ga_{22}Cu_1$	-27	-13	-27	-42
D9	$Ni_{49}Mn_{28}Ga_{22}Co_1$	-	-	-	-
D10	$Ni_{49.5}Mn_{28}Ga_{21.5}V_1$	-	-	-	-
D11	$Ni_{49.5}Mn_{28}Ga_{21.5}Cr_1$	-	-	-	-
D14	$Ni_{49.5}Mn_{28.3}Ga_{21.2}Sb_1$	-33	10	-6	-44
D15	$Ni_{49.5}Mn_{28.3}Ga_{21.2}Sn_1$	-57	-21	-	-
D16	$Ni_{49.5}Mn_{28.3}Ga_{21.2}In_1$	-	-	-	-
D17	$Ni_{49.5}Mn_{28.3}Ga_{21.2}Si_1$	0	12	9	-16
D18	$Ni_{49.5}Mn_{28.3}Ga_{21.2}Ge_1$	-	-	-	-
D19	$Ni_{49.5}Mn_{28.9}Ga_{21.5}B_{0.1}$	2	15	4	-9
D20	$Ni_{54}Mn_{20.9}Ga_{25}B_{0.1}$	17	32	25	6
D21	$Ni_{50}Mn_{25}Ga_{21}Fe_4$	35	58	50	24
D22	$Ni_{50}Mn_{21}Ga_{25}Fe_4$	-	-23	-22	-
A14	$Ni_{47.5}Mn_{32}Ga_{18}Ti_{2.5}$	-	-	-	-

Notes: Transition temperatures outside the range of the instrument are not reported. A_S and A_F represent the austenite start and finish temperature, respectively. M_S and M_F represent martensite start and finish temperature, respectively.

***Table 4**: Curie temperatures (℃) obtained from DSC and TGA and room temperature magnetization.*

sample	composition	DSC		TGA	M (emu/g)
		T_c (H)	T_c (C)	T_c	
D1	$Ni_{49.5}Mn_{28.3}Ga_{21}Fe_{1.2}$	97.7	95.4	93.9	56.1
D2	$Ni_{49}Mn_{26}Ga_{21}Fe_4$	127.6	125.7	122.3	63.5
D3	$Ni_{49}Mn_{20}Ga_{23}Fe_8$	-	-	183	72.2
D4	$Ni_{53}Mn_{23}Ga_{23}Fe_1$	-	-	75.2	49.9
D5	$Ni_{52}Mn_{20}Ga_{24}Fe_4$	115.4	110.0	114.1	64.8
D6	$Ni_{52}Mn_{16}Ga_{24}Fe_8$	111.9	106.8	113.2	50.9
D7	$Ni_{54}Mn_{20}Ga_{25}Fe_1$	39	40	46.3	45.1
D8	$Ni_{49}Mn_{28}Ga_{22}Cu_1$	108.1	103.5	101.8	65.0
D9	$Ni_{49}Mn_{28}Ga_{22}Co_1$	114.0	111.2	111.8	60.9
D10	$Ni_{49.5}Mn_{28}Ga_{21.5}V_1$	111.2	106.3	106.5	58.6
D11	$Ni_{49.5}Mn_{28}Ga_{21.5}Cr_1$	130.0	126.9	127.7	58.0
D14	$Ni_{49.5}Mn_{28.3}Ga_{21.2}Sb_1$	94.6	90.4	90.3	60.6
D15	$Ni_{49.5}Mn_{28.3}Ga_{21.2}Sn_1$	104.0	99.6	98.6	63.9
D16	$Ni_{49.5}Mn_{28.3}Ga_{21.2}In_1$	103.3	98.5	102.2	50.3
D17	$Ni_{49.5}Mn_{28.3}Ga_{21.2}Si_1$	104.1	102.3	99.3	65.6
D18	$Ni_{49.5}Mn_{28.3}Ga_{21.2}Ge_1$	115.3	111.7	112.9	57.6
D19	$Ni_{49.5}Mn_{28.9}Ga_{21.5}B_{0.1}$	103.3	102.2	97.3	62.9
D20	$Ni_{54}Mn_{20.9}Ga_{25}B_{0.1}$	43.9	40.8	38.9	40.3
D21	$Ni_{50}Mn_{25}Ga_{21}Fe_4$	110.2	106.5	111.6	59.4
D22	$Ni_{50}Mn_{21}Ga_{25}Fe_4$	98.2	97.5	92.8	65.5
A14	$Ni_{47.5}Mn_{32}Ga_{18}Ti_{2.5}$	101.1	94.8	97.7	52.6

Notes: Curie temperatures (Tc) are measured from DSC on heating (H) and cooling (C) and from TGA on heating. Room temperature magnetization measured at approximately 0.8 T by vibrating sample magnetometry.

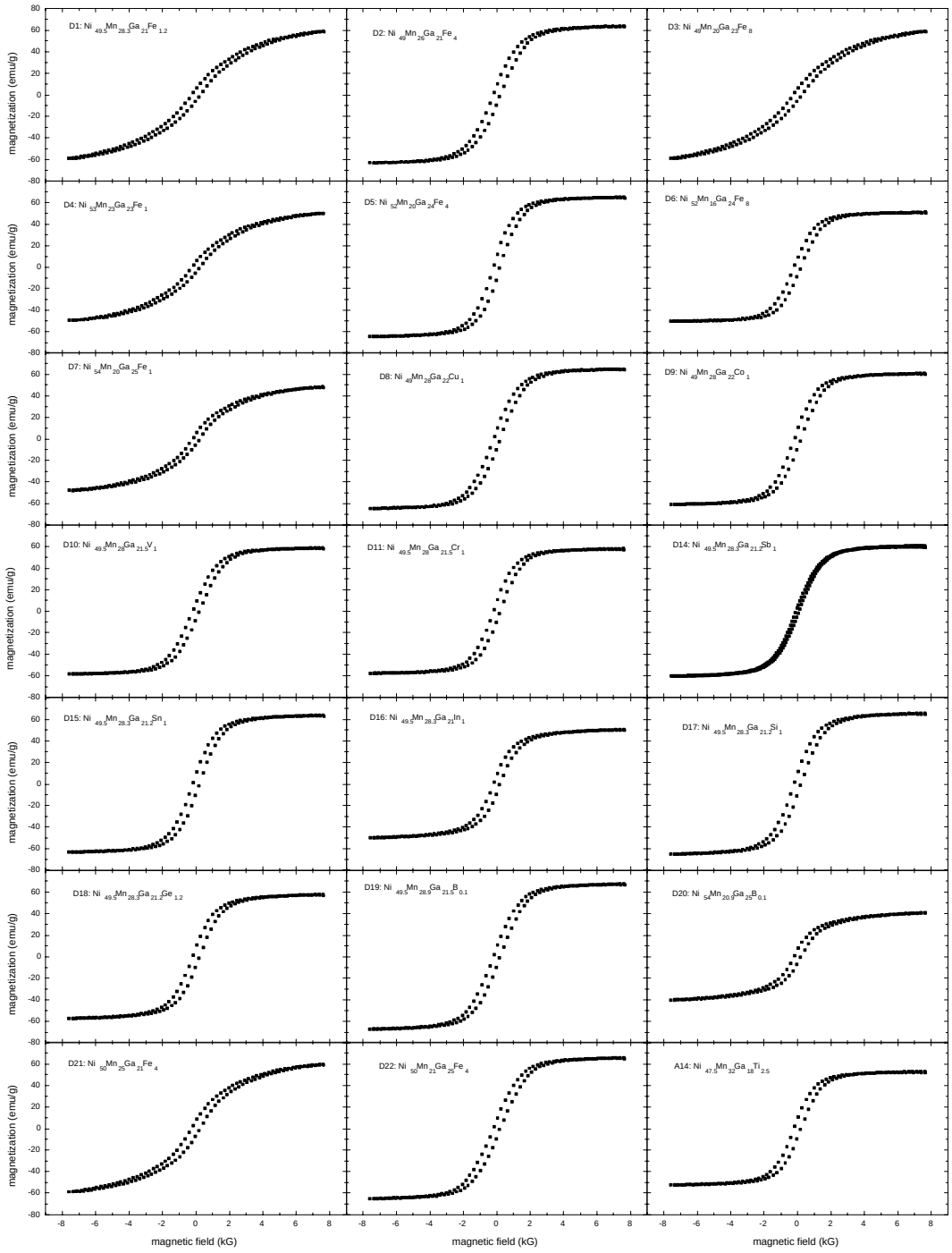

Figure 4: *Room temperature hysteresis loops obtained by vibrating sample magnetization measurements in applied fields up to 0.8 T.*

Typical hysteresis loops at room temperature and low temperature (20 K) as obtained by PPMS measurements are illustrated in Figure 5. These measurements were made for the three samples (D14, D15 and D17) that were considered in detail in the modeling studies. A comparison of results from the VSM and the PPMS are shown in Table 5. This illustrates that the 0.8 T measurements in these cubic samples are very close to saturation. The table also shows that the room temperature VSM and PPMS results at 0.8 T agree quite well. The minor differences are probably due to random weighing errors and some systematic calibration error.

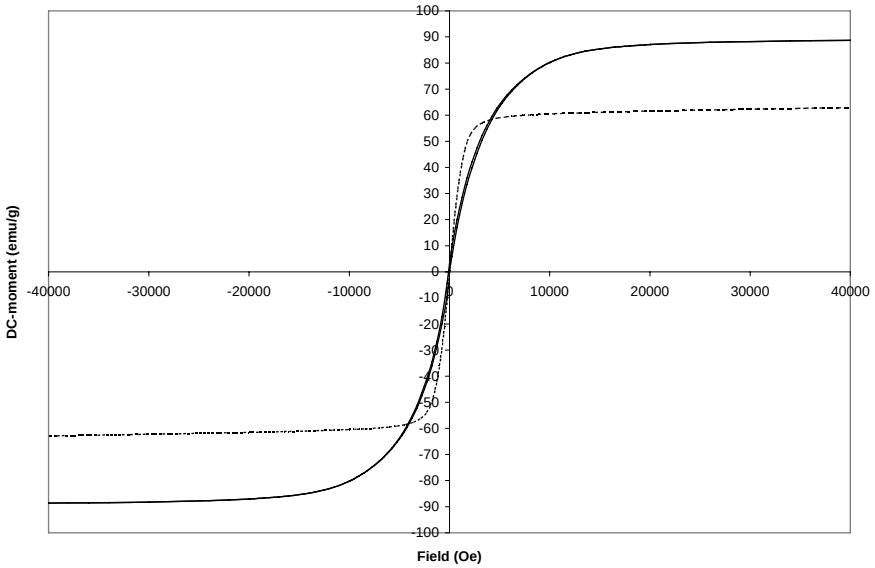

Figure 5: *Room temperature (broken line) and 20 K (solid line) magnetization obtained on the PPMS for sample D14.*

Table 5: *Comparison of magnetizations measured by VSM and PPMS at room temperature (RT) and in different applied fields.*

sample	**composition**	**VSM**	**PPMS**		
		0.8 T (RT)	**0.8 T (RT)**	**4.0 T (RT)**	**4.0 T (20K)**
D14	$Ni_{49.5}Mn_{28.3}Ga_{21.2}Sb_1$	60.5	60.1	62.9	88.6
D15	$Ni_{49.5}Mn_{28.3}Ga_{21.2}Sn_1$	63.9	64.3	67.0	91.7
D17	$Ni_{49.5}Mn_{28.3}Ga_{21.2}Si_1$	65.6	66.9	69.6	93.5

A room temperature ^{57}Fe Mössbauer effect spectrum has been obtained for sample D3 ($Ni_{49}Mn_{20}Ga_{23}Fe_8$) and is illustrated in Figure 6. The spectral lines are broadened, as is

clearly seen in the shape of the outer peaks. The inner lines are much less broadened indicating the presence of multiple Fe sites within the sample. Several possible fitting approaches have been considered based on either Lorentzian or Voigt spectral components.

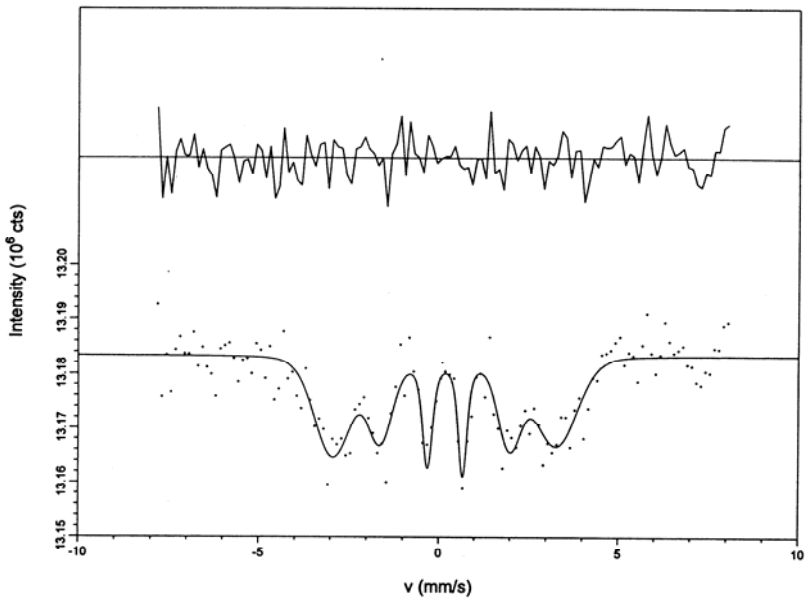

Figure 6: *Room temperature ^{57}Fe Mössbauer effect spectrum of $Ni_{49}Mn_{20}Ga_{23}Fe_8$. The velocity scale is referenced to room temperature α-Fe. The solid line is a computer fit to a Voigt based function with a single component as described in the text and the residuals are shown above the spectrum.*

In the stoichiometric $L2_1$ structure (X_2YZ) there are three discrete crystallographic sites. In the ordered Ni_2MnGa Heusler alloy these sites are occupied by Ni, Mn and Ga, respectively. Substituted Fe in the non-stoichiometric alloy may, in principle, occupy any of these sites, although the composition of the present alloy suggests that Fe may predominantly substitute for Mn. The possibility of three distinguishable Fe sites in this alloy has been considered and in the fits a maximum of three spectral components has been included. The appropriateness of the various fitting methods has been assessed on the basis of the goodness-of-fit, the structure of the residuals and the meaningfulness of the fitted hyperfine parameters.

Goodness of fit parameters for the fits performed here are given in Table 6. The Lorentzian fits show larger values of χ^2 than the Voigt based fits. More substantially, however, is the inability of the Lorentzian fits to properly represent the shape of the spectrum in the region near zero velocity, as illustrated by anomalous features in the residuals. For Voigt based fits the inclusion of more than one component does not significantly improve the goodness-of-fit and the fitted intensity of the additional components is sufficiently small that it has no substantial effect on the shape of the hyperfine field distribution or the mean hyperfine parameters. On the basis of this analysis it is established that the most meaningful fit to the spectrum obtained here is a fit to a single Voigt based function. This is illustrated in

Figure 6. The hyperfine field distribution obtained from this Mössbauer effect spectrum is illustrated in Figure 7. Mean hyperfine parameters are given in Table 7.

Table 6: *Goodness-of-fit parameters (χ^2) for various fits to the spectrum shown in Figure 6.*

model	**components**	χ^2
Lorentzian	1	1.53
	2	1.32
	3	1.11
Voigt	1	1.06
	2	1.05
	3	1.01

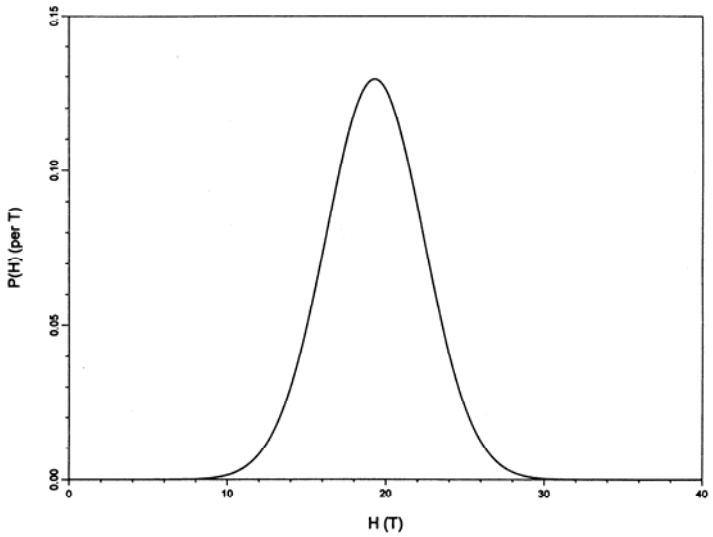

Figure 7: *Fe hyperfine field distribution as obtained from the room temperature ^{57}Fe Mössbauer effect spectrum of $Ni_{49}Mn_{20}Ga_{23}Fe_8$.*

***Table 7**: Mean Fe hyperfine parameters for $Ni_{49}Mn_{20}Ga_{23}Fe_8$.*

parameter	**symbol**	**units**	**value**
center shift	$<\delta>$	mm/s	+0.17(1)
quadrupole shift	$<\varepsilon>$	mm/s	-0.003(3)
hyperfine field	$<\|H\|>$	T	19.3(5)
Gaussian width	σ	T	3.1(5)

Notes: Estimated uncertainties are given for the least significant digit in ( ). The center shift is referenced to room temperature α-Fe.

The measured center shifts may be compared with center shifts from the literature for dilute Fe alloys. These are shown in Table 8. These shifts may be viewed in the context of the neighbor environment around an Fe ion that substitutes for Mn in the $L2_1$ structure (Table 9). These neighbor locations are obtained from the more general structural information presented in Annex 1. The measured center shift value is consistent with expectations for Fe with Ni nearest neighbors and Ga second nearest neighbors and follows from the assumption that Fe substitutes primarily for Mn in the $L2_1$ structure. The large negative center shift from the large electron density around Mn ions has less influence in the present situation because of the greater Fe-Mn distances (Table 9).

***Table 8:** Measured room temperature center shifts for dilute Fe in various hosts referenced to α-Fe (from the literature).*

host	**center shift**
Ni	+0.020
Mn	-0.230
Ga	+0.375

The small observed quadrupole splitting is consistent with the high degree of symmetry surrounding the Mn sites in the $L2_1$ structure. The local hyperfine field at a nucleus in a ferromagnetic material has potential contributions from the presence of a local magnetic moment on the probe atom and a transferred field from neighboring moments. In the present case the details of the local moments carried by Fe ions are unknown although the presence of ferromagnetism in the $D0_3$ phase of Fe_3Ga suggests the likelihood of local moment formation. It is, however, probable that the local Fe field is, to a large extent, a transferred field resulting from large localized moments on the third nearest neighbor Mn atoms.

The present analysis does not indicate the presence of distinct Fe environments as would result from chemical ordering of the substitutional Fe atoms. Rather the broad, single

component field distribution suggests the random substitution of Fe on the Mn sites as well as the intrinsic disorder associated with the non-stoichiometric composition of this alloy.

Table 9: *Nearest neighbor shells around an Fe atom substituting for Mn (Y-sites) in the stoichiometric Ni_2MnGa Heusler structure.*

shell	**distance (r/a)**	**neighbors**
1	0.433	8Ni
2	0.500	6Ga
3	0.707	12Mn
4	0.829	24Ni
5	0.866	8Ga
6	1.000	6Mn

3. Discussion of Experimental Results

The results obtained here allow for several conclusions to be drawn concerning the effects of composition and alloying additions on the properties of Ni-Mn-Ga Heusler alloys that are relevant to their use as magnetic shape memory alloys. The particular factors that are of most significance are the austenite and martensite transition temperatures, the Curie temperature and the saturation magnetization. For practical applications it is important to have structural and magnetic transition temperatures as far above room temperature as possible and to have as large a room temperature saturation magnetization as possible. Although not addressed in this study, maximization of both the magnetic field induced strain and stress-induced strain is key for development of magnetic shape memory alloys.

The structural transition temperatures, as summarized in Table 3, are highest for those compositions that contain a small amount of Fe (e.g., samples D1, D4, D21). Closer examination of the results shows that the high temperatures may be correlated with high Mn content (near 25 at%). Alloys with lower Mn content (e.g., samples D3, D5, D6, D22) tend to have much lower structural transformation temperatures; structural transformation temperatures for samples D3, D5 and D22 were below the instrumental limits (near 80C). Table 4 shows some correlation between structural transition temperature and Curie temperature. Although, Curie temperatures for the Fe containing compositions with the highest structural transition temperatures are not the highest of the alloys studied here, they are, in general, sufficiently above room temperature to indicate a correlation. A comparison of the Curie temperatures of the alloys that show the highest structural transition temperatures show trends that are expected on the basis of a detailed consideration of the magnetic interactions in the Heusler phase. Alloys with Mn contents that deviate from the Heusler stoichiometry (either above or below 25 at%), have lower Curie temperatures. This is discussed further with regard to magnetic interactions in these alloys in the next sections. The trends that result from varying Fe content in the alloys is less clear as a comparison of D2 and D3 suggests increasing Fe content increases the Curie temperature, while a comparison of D5 and D6 does not support this trend.

The room temperature magnetization depends on the intrinsic (low temperature) saturation magnetization, the relationship of room temperature and the Curie temperature and the degree to which the sample is magnetically saturated in the measuring field. While compositional trends are difficult to define clearly because of the interrelationship of these factors, the effect of Curie temperature is quite obvious. There is a direct correspondence between room temperature magnetization and Curie temperature for D20 and D7, which have the lowest Curie temperatures and D3 which has the highest Curie temperature.

The low temperature magnetization measurements will be discussed in detail in the next sections.

4. Modelling Approach

4.1 The Indirect Exchange Model

The magnetic properties of the Heusler alloys (and similar materials) are the result of an indirect exchange interaction between localized magnetic moments. This interaction is important in metals where the magnetic moments are sufficiently far apart to preclude the existence of a direct exchange coupling. The indirect exchange interaction is the result of the polarization of the conduction band and is well described by the so-called RKKY (Ruderman-Kittel-Kasuya-Yosida) oscillations [9,10]. The physical properties of the system that are most relevant in this approach are the spatial distribution of the localized magnetic moments, the magnitude of these moments and the overall conduction electron density. The oscillatory nature of the interaction is significant as both the magnitude and the sign of the exchange coupling is radially dependent. The application of indirect exchange interactions to ferromagnetic materials has been described by several authors [11-21]. These concepts have been shown to be appropriate for the description of Heusler and related alloys [13-15,22-25].

The radial dependence of the conduction electron polarization, $p(r)$, around a localized unit magnetic moment in a free electron gas is given by [13-15,19-20]

$$p(r) = -\frac{5}{4\pi^2 r^3}\left[\sin\delta_d^{\uparrow}\cos(2k_F r + \delta_d^{\uparrow} + \frac{\eta}{r}) - \sin\delta_d^{\downarrow}\cos(2k_F r + \delta_d^{\downarrow} + \frac{\eta}{r})\right]. \quad (1)$$

Here k_F is the Fermi wave vector given by

$$k_F = \frac{1}{a}\left[48\pi^2 n_0\right]^{1/3} \quad (2)$$

where a is the lattice parameter and n_0 is the average conduction electron contribution per atom in the material. In equation (1) δ_d^{σ} is the d-wave phase shift for electrons of spin σ. For an ion that contributes Z_{sp} electrons to the conduction band, δ_d^{σ} is related to the average conduction electron contribution as

$$\delta_d^{\sigma} = \frac{8}{\pi}\left[Z_{sp} - n_0\right] \quad (3)$$

In the above η is a preasymptotic phase factor as given by Jena and Geldart [13-15];

$$\eta = \frac{\pi a}{4}. \tag{4}$$

The calculation of n_0 follows from a consideration of the electronic structure of the component ions in the alloy. The number of electrons contributed to the conduction band from each ion has been considered extensively for the Heusler alloys [22-25] and it is important to note that this is not the same as the number of electrons that is commonly used to estimate the structural stability of these alloys [1-2]. The average conduction electron contribution per atom in an alloy of the composition $Ni_xMn_yGa_zZ_\alpha$ (x+y+z+α = 100) in terms of the conduction electron contributions from the different elemental components is

$$n_0 = \frac{1}{100}\left[\mathrm{x}n(\mathrm{Ni}) + \mathrm{y}n(\mathrm{Mn}) + \mathrm{z}n(\mathrm{Ga}) + \alpha n(\mathrm{Z})\right]. \tag{5}$$

The determination of the conduction electron contributions from each of the elements is not unambiguous but may be considered in terms of the known behavior of stoichiometric Heusler alloys within the context of the rigid band approximation. An important factor in this calculation is the location and magnitude of the magnetic moments in the system. It can be readily shown that as long as the number of spin down electrons on each ion does not change, that the redistribution of magnetic moments in the system does not alter the average conduction electron contribution per atom. However, the location of the moments in the system and their orientation will influence the overall magnetic properties of the material. The conduction electron contributions of the ions as well as the determination of δ_d^σ are discussed in the next section.

From the above discussion and following the development of Geldart and Ganguly [18] and Malmstrom et al. [19,20], the interaction energy between two spins, *i* and *j* is given by

$$E_{ij}(r) = \frac{25\varepsilon_F}{2\pi^2 S_i S_j} \sin\delta_{di}^{\downarrow} \sin\delta_{dj}^{\downarrow} \frac{\cos\left(2k_F r + \delta_{di}^{\downarrow} + \delta_{dj}^{\downarrow} + \dfrac{\eta}{r}\right)}{\left(k_F r\right)^3} \tag{6}$$

where ε_F is the Fermi energy.

4.2 Application of the indirect exchange model

The application of the indirect exchange model as described above requires a knowledge of a number of material's parameters. Specifically the parameters that are required are:

i) the lattice parameter,

ii) the composition of the alloy,

iii) the distribution of magnetic moments on the lattice sites,

iv) the magnetic moment associated with each type of atom and

v) the conduction electron contribution from each type of atom.

Some parameters, such as the lattice parameter can be measured directly and have been given above in the experimental section. Other parameters, such as the magnitude and distribution of magnetic moments in the system can be determined on the basis of certain assumptions subject to their consistency with measured quantities. Yet other parameters, such as the conduction electron contribution of each element are determined from assumptions involving a general knowledge of electronic structure and are not directly related to measured properties of the present alloys.

Our ability to apply the model as described above to the experimental results requires the selection of alloys from those studied here that facilitate the implementation of the model. The criteria that we have used are as follows:

i) cubic structure at room temperature

ii) reasonable knowledge of the distribution of magnetic moments in the system and

iii) reasonable ability to determine the conduction electron contributions of the atoms.

On the basis of these criteria we have focused our attention on alloys D14, D15 and D17 that are of the form $Ni_{49.5}Mn_{28.3}Ga_{21.2}Z_1$ (Z = Sb, Sn and Si, respectively). For these alloys the required parameters as described above are determined as follows:

i) The lattice parameter has been measured by x-ray diffraction and is given in Table 2.

ii) The composition of the alloys has been taken as the starting composition of each ingot as indicated in Table 1.

iii) The distribution of magnetic moments on the lattice sites results from the distribution of Mn and Ni ions on the lattice. Details of the neighbor configurations in the cubic Heusler structure are discussed in detail in Annex 1. As the alloys investigated here have excess Mn, it is assumed that the Y sites in the X_2YZ $L2_1$ structure are fully occupied with Mn. As the Ni composition is only slightly less that the stoichiometric Heusler composition it is also assumed that all Ni occupies X sites and the excess Mn resides on the Z sites (normally occupied by Ga, which is deficient in the present alloys). Enkovaara et al. [7] have speculated that the excess Mn on Ga sites couples antiferromagnetically with the Mn residing on the Mn sites and that the small Ni moments couple ferromagnetically with the Y site Mn. This hypothesis is demonstrated to be true on the basis of a fundamental analysis of the magnetic interactions in these alloys in the present work.

iv) The magnitude of the moment associated with each Mn ion is determined from the measured low temperature magnetization of each sample as obtained using the PPMS and the above assumptions concerning the location and orientation of the magnetic moments. This calculation is described in Annex 2.

v) The conduction electron contribution from each type of atom is determined using guidelines from the literature on work concerning magnetic interactions in Heusler alloys as follow:

Nickel: Mayo and Dunlap [24] have suggested a conduction band contribution of 0.1 electrons per Ni atom in Heusler alloys. This value has provided excellent agreement with hyperfine field systematics in Ni_2MnGa.

Manganese: The localized magnetic moment, μ(Mn), associated with a Mn ion is given (in μ_B) as the difference in the number of spin up d-electrons, $Z_d^{\uparrow}$, and the number of spin down d-electrons, $Z_d^{\downarrow}$, as

$$\mu = Z_d^{\uparrow} - Z_d^{\downarrow} \tag{7}$$

and corresponds to a net Mn spin of $S = \mu/2$. For Mn (electron configuration $[Ar]3d^5 4s^2$) the Friedel sum rule [17] gives

$$Z_{sp} + Z_d^{\uparrow} + Z_d^{\downarrow} = 7 \tag{8}$$

where the conduction band contribution per Mn ion is given by Z_{sp}. Caroli and Blandin [16] have considered the simple assumption that in cases where the magnetic moment is large then one sub-band is filled [e.g. $Z_d^{\uparrow}$=5]. However, for Ni_2MnGa and related Heusler alloys, Jha et al. [25] have suggested that $Z_d^{\uparrow}$=4.5 is more appropriate and have shown that this provides good agreement with experiment for a variety of hyperfine magnetic fields in a variety of different Heusler hosts. Combining equations (7) and (8) gives

$$Z_{sp} = \mu - 2 \tag{9}$$

Gallium, Silicon, Tin and Antimony: For these atoms the standard sp electron configuration has been assumed; $[Ar]3d^{10}4s^24p^1$, $[Ne]3s^23p^2$, $[Kr]4d^{10}5s^25p^2$ and $[Kr]4d^{10}5s^25p^3$, for Ga, Si, Sn and Sb, respectively. This gives the number of contributed conduction electrons as n(Ga) = 3, n(Si) = 4, n(Sn) = 4 and n(Sb) = 5.

The calculation of the conduction electron contribution from Mn follows from a measurement of the Mn magnetic moment. For samples D14, D15 and D17 this is obtained from low temperature magnetization measurements as discussed in Annex 2. The interpretation of these results follow from the fact that neutron diffraction studies have shown that Ni carries a small magnetic moment (about 0.24 μ_B) [26]. The current discussion in Annex 2 as well as calculations presented in the literature [7] show that such a Ni moment is necessary in order to provide an overall consistent picture of the observed magnetic properties of these alloys. It is, therefore, necessary to consider Mn-Ni exchange coupling as well as Mn-Mn coupling. The Ni-Ni coupling will be weak as a result of the small localized Ni moment. Following the methodology of Malmstrom, Geldart and Blomberg [19,20] as summarized in equation (6), the indirect exchange coupling between unlike ions can be calculated in the context of RKKY theory.

Using the parameters as described above, the exchange coupling energy as a function of distance for Mn-Mn and Mn-Ni interactions has been calculated for the $L2_1$ Heusler structure is illustrated in Figure 8. The interaction between nearest neighbor magnetic moments within the first unit cell is determined on the basis of the atomic distances given in Table 10. An inspection of Figure 8 shows the following signs for the exchange coupling of Mn and Mn or Ni on different lattice sites:

Mn(Y)-Mn(Y) - positive

Mn(Y)-Mn(Z) - negative

Mn(Y)-Ni(X) – positive

Table 10: *Interatomic distances in units of r/a for the $L2_1$ Heusler structure.*

lattice sites	**distance (r/a)**
Y-X	0.433
Y-Y	0.707
Y-Z	0.500

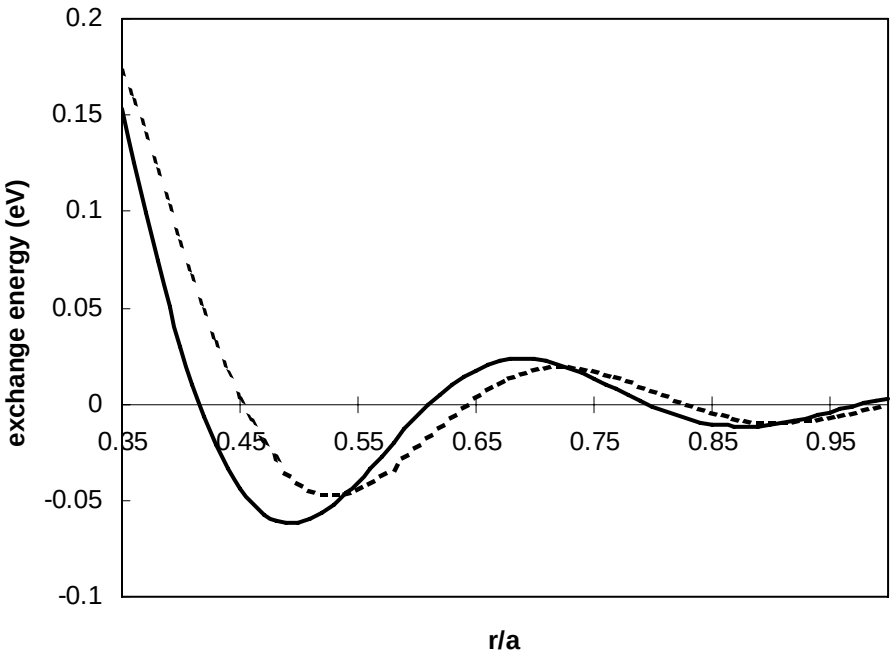

Figure 8: *Exchange coupling energy as a function of distance for Mn-Mn coupling (solid line) and Mn-Ni coupling (broken line).*

These results show that Mn on the Heusler Y sites will couple ferromagnetically (positive exchange coupling) with other Mn on Y sites, antiferromagnetically (negative exchange) with Mn on Z sites and ferromagnetically with Ni on X sites. This coupling confirms the interpretation of the magnetization measurements of our samples D14, D15 and D17 in terms of the assignment of moments to the Mn and Ni ions. The calculation above confirms the magnetic order that exists in these alloys and provides a firm theoretical basis for the interpretation of magnetization measurement.

5. Conclusions and suggestions for future work

The experimental studies presented here have provided both a methodology for the preliminary evaluation of Ni-Mn-Ga based ferromagnetic shape memory alloys as well as guidelines for compositions on which to pursue further more detailed investigations. Specifically, alloys which contain up to a few percent Fe seem to show promise and the study of alloys of the form $Ni_xMn_yGa_zFe_\alpha$ for $x \cong 50$, $y \cong 25\text{-}29$, $z \cong 21\text{-}22$ and $\alpha \cong 1 - 4$ at% would be beneficial. These studies may proceed by means of combinatorial materials science methods and for this purpose the development and refinement of techniques for the measurement of relevant properties of such films is important. The ability to structurally characterize these combinatorial films exists at Dalhousie University and has been utilized for previous DRDC work. In principle, facilities for investigating the magnetization of these films are available at Dalhousie University and procedures for effectively implementing these techniques need to be developed. Finally the ability of thermal analysis techniques (DSC and TGA) to study combinatorial films for the purpose of obtaining structural transition temperatures needs to be determined. This could utilize facilities at DRDC or at Dalhousie. Once compositions of interest are clearly defined further work would, undoubtedly, involve the growth and investigation of oriented single crystals. Single crystals could be characterized using well established techniques at DRDC (Laue diffraction, TGA, DSC, etc.). The relatively small number of reasonably massive samples would be amenable to investigation using the PPMS at the Institute for Research on Materials and the VSM at Dalhousie as well as the torque magnetometer at DRDC.

Theoretical studies have clarified the fundamental interactions that are responsible for the magnetic behavior of these alloys. The reasons for combined ferromagnetic and antiferromagnetic order in these alloys and the relationship of the individual magnetic moments to the overall magnetization have been described on the basis of indirect exchange coupling. In the context of the proposed extensions to the experimental work as discussed above, the application of these theoretical concepts to Fe-containing alloys can be an important factor in understanding the relationship of the Fe magnetic moment to the overall properties of the alloy. This application will be particularly meaningful in the case of combinatorial studies as the continuous range of sample compositions will allow for a detailed systematic investigation.

6. References

[1] S.K. Wu and S.T. Wang, Materials Lett. 57 (2003) 4291.

[2] N. Lanska, O. Söderberg, A. Sozinov, Y. Ge, K. Ullakko and V.K. Lindroos, J. Appl. Phys. 95 (2004) 8074.

[3] V.V. Khovailo, V.A. Chernenko, A.A. Cherechukin, T. Takagi and T. Abe, J. Magn. Magn. Mater. 272-274 (2004) 2067.

[4] O. Söderberg, K. Koho, T. Sammi, X.W. Liu, A. Sozinov, N. Lanska and V.K. Lindroos, Mater. Sci. Engg. A 378 (2004) 389.

[5] K. Koho, O. Söderberg, N. Lanska, Y. Ge, X. Liu, L. Straka, J. Vimpari, O. Heczko and V.K. Lindroos, Mater. Sci. Engg. A 378 (2004) 384.

[6] T. Kanomata, K. Shirakawa and T. Kaneko, J. Magn. Magn. Mater. 65 (1987) 76.

[7] J. Enkovaara, O. Heczko, A. Ayuela, L. Nordstrom and R.M. Nieminen, Phys. Rev. B 67 (2003) 212405.

[8] TA Instruments, Inc., Technical note TS-37 (http://www.tainst.com).

[9] C. Kittel. Introduction to Solid State Physics, 7th ed. (Wiley, New York, 1996) p. 628.

[10] R.M. White, Quantum Theory of Magnetism (McGraw-Hill, New York 1970) p. 197-200.

[11] A. Blandin and I.A. Campbell, Phys. Rev. Lett. 31 (1973) 51.

[12] I.A. Campbell and A. Blandin, J. Magn. Magn. Mater. 1 (1975) 1.

[13] P. Jena and D.J.W. Geldart, Phys. Rev. B 7 (1973) 439.

[14] P. Jena and D.J.W. Geldart, Solid State Commun. 15 (1974) 139.

[15] P. Jena and D.J.W. Geldart, J. Magn. Magn. Mater. 8 (1978) 99.

[16] B. Caroli and A. Blandin, J. Phys. Chem. Solids 27 (1966) 503.

[17] J. Friedel, Phil. Mag. 43 (1952) 153.

[18] D.J.W. Geldart and P. K. Ganguly, Phys. Rev. B 1 (1970) 3101.

[19] G. Malmstrom, D.J.W. Geldart and C. Blomberg J. Phys. F: Metal Phys. 6 (1976) 233.

[20] G. Malmstrom, D.J.W. Geldart and C. Blomberg, J. Phys. F: Metal Phys. 6 (1976) 1953.

[21] J. Reitz and M.B. Stearns, J. Appl. Phys. 50 (1979) 2066-2068.

[22] R.A. Dunlap and G. Stroink, Can. J. Phys. 60 (1982) 909.

[23] R.A. Dunlap and D.F. Jones, Phys. Rev. B 26 (1982) 6013.

[24] W.R. Mayo and R.A. Dunlap, J. Appl. Phys. 52 (1982) 8082.

[25] S. Jha, H.M. Seyoum, G.M. Julian, M. deMarco, G.K. Shenoy and R.A. Dunlap, Phys. Rev. B 32 (1985) 6104.

[26] P.J. Brown, A.Y. Bargawi, J. Crangle, K.U. Neumann and K.R.A. Ziebeck, J. Phys. Condensed Matter **11** (1999) 4715.

[27] P.J. Webster, The Magnetic and Chemical Structures of Heusler Alloys, Ph.D. Thesis, University of Sheffield (1968).

Annex 1: Neighbor coordination in the cubic $L2_1$ Heusler structure

The four sites (ABCD) in the ordered cubic $L2_1$ Heusler structure with the stoichiometric X_2YZ composition contain the X ions in the A and C sites, Y ions in the B site and Z ions in the D site. This structure is illustrated in Figure A1.

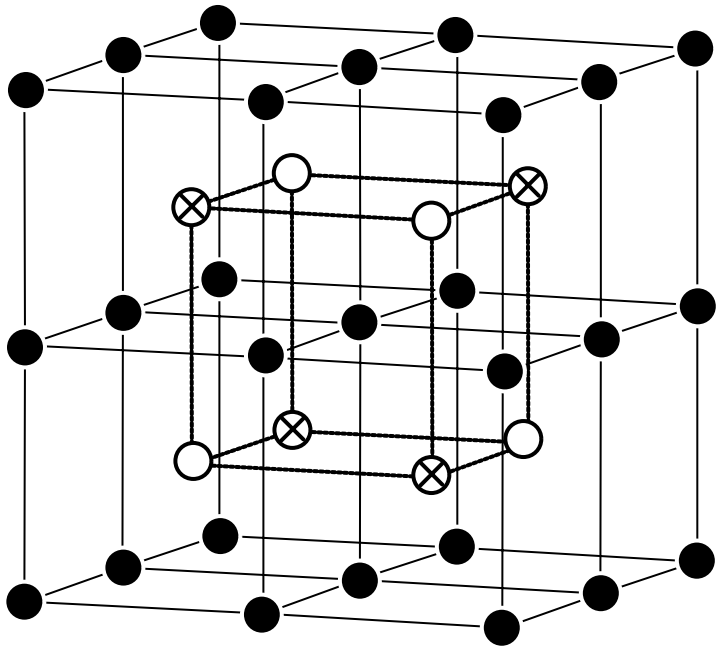

Figure A1: *The $L2_1$ Heusler structure (● = A- and C-sites, ⊗ = B-sites, ○ = D-sites). In the stoichiometric X_2YZ phase the site occupancy is A- and C-sites (Ni), B-sites (Mn) and C-sites (Ga).*

In the present work we are primarily concerned with calculating the interactions as seen by the Mn ions. These are located primarily on the Y sites with excess Mn residing on the Z sites (as discussed in the text). The neighbor shells for Mn on the Y sites are given in Table A1. Neighbor shells for other sites are found by cyclic permutations of the neighbor configurations (A→B→C→D→A etc).

Table A1: *Neighbor shells for the B sites of the ABCD ($L2_1$) structure. Directions vectors are given in terms of the unit length a/4. Shells up to a radius of ($100^{1/3}$)*r(3nn) are given.*

shell	h k l	$h^2+k^2+l^2$	r/a	coordination	neighbors
1	1 1 1	3	0.433013	8	4A, 4C
2	0 0 2	4	0.500000	6	6D
3	0 2 2	8	0.707107	12	12B
4	1 1 3	11	0.829156	24	12A, 12C
5	2 2 2	12	0.866025	8	8D
6	0 0 4	16	1.000000	6	6B
7	1 3 3	19	1.089724	24	12A, 12C
8	0 2 4	20	1.118034	24	24D
9	2 2 4	24	1.224745	24	24B
10	1 1 5, 3 3 3	27	1.299038	32	16A, 16C
11	0 4 4	32	1.414214	12	12B
12	1 3 5	35	1.479020	48	24A, 24C
13	0 0 6, 2 2 4	36	1.500000	30	30D
14	0 2 6	40	1.581139	24	24B
15	3 3 5	43	1.639360	24	12A, 12C
16	2 2 6	44	1.658312	24	24D
17	4 4 4	48	1.732051	8	8B
18	1 1 7, 1 5 5	51	1.785357	48	24A, 24C
19	0 4 6	52	1.802776	24	24D
20	2 4 6	56	1.870829	48	48B
21	3 5 5, 1 3 7	59	1.920286	72	36A, 36C
22	0 0 8	64	2.000000	6	6B
23	3 3 7	67	2.046338	24	12A, 12C
24	4 4 6, 0 2 8	68	2.061553	48	48D
25	2 2 8, 0 6 6	72	2.121320	36	36B
26	5 5 5, 1 5 7	75	2.165063	56	28A, 28C
27	2 6 6	76	2.179449	24	24D
28	0 4 8	80	2.236068	24	24B

29	3 5 7, 1 1 9	83	2.277608	72	36A, 36C
30	2 4 8	84	2.291288	48	48D
31	4 6 6	88	2.345208	24	24B
32	1 3 9	91	2.384848	48	24A, 24C
33	4 4 8	96	2.449490	24	24B
34	3 3 9, 1 7 7, 5 5 7	99	2.487469	72	36A, 36C
35	0 6 8, 0 0 10	100	2.500000	30	30D
36	0 2 10, 2 6 8	104	2.549510	72	72B
37	1 5 9, 3 7 7	107	2.586020	72	36A,C36
38	6 6 6, 2 2 10	108	2.598076	32	32D
39	3 5 9	115	2.680951	48	24A, 24C
40	4 6 8, 0 4 10	116	2.692582	72	72D
41	2 4 10	120	2.738613	48	48B
42	1 1 11, 5 7 7	123	2.772634	48	24A, 24C
43	0 8 8	128	2.828427	8	8B
44	1 7 9, 5 5 9, 1 3 11	131	2.861381	120	60A, 60C
45	2 8 8, 4 4 10	132	2.872281	48	48D
46	6 6 8, 0 6 10	136	2.915476	48	48B
47	3 7 9, 3 3 11	139	2.947457	72	36A, 36C
48	2 6 10	140	2.958040	48	48D
49	0 0 12, 4 8 8	144	3.000000	30	30B
50	1 5 11, 7 7 7	147	3.031089	56	28A, 28C
51	0 2 12	148	3.041381	24	24D
52	2 2 12, 4 6 10	152	3.082207	72	72B
53	3 5 11, 5 7 9	155	3.112475	96	48A, 48C
54	0 4 12	160	3.162278	24	24B
55	1 9 9	163	3.191786	24	12A, 12C
56	0 8 10, 2 4 12, 6 8 8	164	3.201562	96	96D
57	2 8 10	168	3.240370	48	48B
58	3 9 9, 1 7 11, 5 5 11, 1 1 13	171	3.269174	120	60A, 60C
59	6 6 10	172	3.278719	24	24D

Annex 2: Magnetic units and the calculation of magnetic moments.

The bulk magnetization of a sample is given by the vector sum of the individual magnetic moments associated with the ions as

$$\vec{M} = \sum \vec{\mu} \tag{A2.1}$$

The total magnetization is, therefore, measured in the same units as the individual magnetic moments. The magnetization may also be expressed as a quantity per unit volume. In the case of a saturated ferromagnetic material with a single type of moment carrying site, this may be expressed as

$$M = N\mu \tag{A2.2}$$

Where N is the number of magnetic moment carrying ions per unit volume. In our present measurements the magnetization per unit mass has been obtained. Thus N in equation (A2.2) is the number of moment carrying ions per unit mass. The magnetization per unit mass obtained from both the VSM and PPMS measurements is expressed in emu/g. This is identical to the SI unit for magnetization per unit mass:

$$1\frac{emu}{g} = 1\frac{A \cdot m^2}{kg} \tag{A2.3}$$

Magnetization values found in the literature are sometimes expressed in units of Gauss. The magnetization in Gauss is related to the magnetization in emu/g through the density as

$$M(G) = M\left(\frac{emu}{g}\right) \times \rho\left(\frac{g}{cm^3}\right) \tag{A2.4}$$

For example for Ni at room temperature (as has been used as a standard for the present work);

$$485G = 54.43\frac{emu}{g} \times 8.91\frac{g}{cm^3} \tag{A2.5}$$

The magnetic moment per ion may be obtained from equation (A2.2). It is convenient to express this as

$$\mu = \frac{MA}{N_A \mu_B} \tag{A2.6}$$

where A is the atomic weight, N_A is Avogadro's number and μ_B is the Bohr magneton. Expressing M in units of emu/g and $\mu_B = 9.27\times10^{-21}$ erg/G will give a moment per ion in units of the Bohr magneton. For Ni at low temperature this is

$$\frac{57.24 \times 58.71}{6.02\times10^{23} \times 9.27 \times 10^{-21}} = 0.602\mu_B . \tag{A2.7}$$

In the case of the cubic Heusler phase alloys of composition $Ni_xMn_yGa_zZ_\delta$, where $x+y+z+\delta=100$ and a unit cell as described by the lattice parameters given in Table 2, the unit cell, which contains a total of 16 atoms, will contain x/6.25 Ni atoms, y/6.25 Mn atoms, z/6.25 Ga atoms and δ/6.25 Z atoms. The mass of this unit cell (in grams) will be given as

$$m\left(\frac{g}{cell}\right) = \frac{1}{6.25N_A}\left[xA_{Ni} + yA_{Mn} + zA_{Ga} + \delta A_z\right] \tag{A2.8}$$

where the A_i are the atomic weights of the elemental components. The magnetization per unit cell may be expressed in terms of the measured magnetization per gram as

$$M\left(\frac{emu}{cell}\right) = M\left(\frac{emu}{g}\right) \times m\left(\frac{g}{cell}\right) \tag{A2.9}$$

From equation (A2.6) this gives the moment per cell in Bohr magnetons as

$$\mu = \frac{M\left(\frac{emu}{cell}\right)}{\mu_B} \tag{A2.10}$$

On the basis of the hypothesis of Enkovaara et al. [7] and the results of the present calculations, it is assumed that the 4 Mn ions per cell that reside on the Y sites have moments that will align in one direction while the remaining (y-25)/6.25 Mn ions per unit cell that reside on the Z sites have moments that will align in the opposite direction. Furthermore, Brown et al. [26] have reported that the Ni ions carry a magnetic moment of 0.24 μ_B that couples ferromagnetically to the Mn(Y) moments (this is discussed further in the text). This gives rise to (50-y)/6.25 net Mn ions and 49.5/6.25 Ni ions that contribute to the overall magnetization per unit cell. For the present alloys y = 28.3 so the magnetization per unit cell arises as a result of (50-28.3)/6.25 = 3.472 unpaired Mn spins and 7.92 Ni spins. These data provide the magnetic moments as given in Table A2. These results are consistent with Enkovaara et al.'s [7] assumption of 3.5 μ_B per Mn and Webster's [27] measured value of 4.17 μ_B per Mn for the stoichiometric Heusler composition.

***Table A2**: Magnetic moment per Mn ion as calculated from the measured low temperature magnetization for $Ni_{49.5}Mn_{28.3}Ga_{21.2}Z_1$. It is assumed tat the Ni moment is the same (0.24 μ_B) in all alloys.*

sample	Z	M (emu/g)	m (g/cell)	M (emu/cell)	μ/cell (μ_B)	μ/Mn (μ_B)
D14	Sb	88.6	1.6100×10^{-21}	1.426×10^{-19}	15.38	3.88
D15	Sn	91.7	1.6092×10^{-21}	1.476×10^{-19}	15.92	4.03
D17	Si	93.5	1.5851×10^{-21}	1.482×10^{-19}	15.99	4.06

Distribution list

DRDC Atlantic CR 2006-042

LIST PART 1: Internal Distribution by Centre

Hard Copies	Electronic Copies	
1	4	DRDC Atlantic Library
2	2	Shannon Farrell
1	1	Leon Cheng
1	1	Calvin Hyatt
1	0	Allison Nolting
6	8	TOTAL LIST PART 1

LIST PART 2: External Distribution by DRDKIM

Hard Copies	Electronic Copies	
0	1	DRDC/DRDKIM
2	1	Richard A. Dunlap Weathervane Scientific Incorporated P.O. Box 31030 Halifax, NS B3K 5T9
2	2	TOTAL LIST PART 2
8	10	TOTAL COPIES REQUIRED

This page intentionally left blank.

DOCUMENT CONTROL DATA

(Security classification of title, body of abstract and indexing annotation must be entered when the overall document is classified)

1. ORIGINATOR (the name and address of the organization preparing the document.. Organizations for whom the document was prepared, e.g. Centre sponsoring a contractor's report, or tasking agency, are entered in section 8.)

Weathervane Scientific Incorporated
P.O. Box 31030,
Halifax, NS B3K 5T9

2. SECURITY CLASSIFICATION (overall security classification of the document including special warning terms if applicable).

UNCLASSIFIED

3. TITLE (the complete document title as indicated on the title page. Its classification should be indicated by the appropriate abbreviation (S,C,R or U) in parentheses after the title).

Effects of composition on the properties of magnetic shape memory alloys.

4. AUTHORS (Last name, first name, middle initial. If military, show rank, e.g. Doe, Maj. John E.)

Richard A. Dunlap

5. DATE OF PUBLICATION (month and year of publication of document)

March 2007

6a. NO .OF PAGES (total containing information Include Annexes, Appendices, etc).

30

6b. NO. OF REFS (total cited in document)

27

7. DESCRIPTIVE NOTES (the category of the document, e.g. technical report, technical note or memorandum. If appropriate, enter the type of report, e.g. interim, progress, summary, annual or final. Give the inclusive dates when a specific reporting period is covered).

CONTRACT REPORT

8. SPONSORING ACTIVITY (the name of the department project office or laboratory sponsoring the research and development. Include address).

Defence R&D Canada – Atlantic
PO Box 1012
Dartmouth, NS, Canada B2Y 3Z7

9a. PROJECT OR GRANT NO. (if appropriate, the applicable research and development project or grant number under which the document was written. Please specify whether project or grant).

11gm19

9b. CONTRACT NO. (if appropriate, the applicable number under which the document was written).

W7707-042846/001/HAL

10a ORIGINATOR'S DOCUMENT NUMBER (the official document number by which the document is identified by the originating activity. This number must be unique to this document.)

DRDC Atlantic CR 2006-042

10b OTHER DOCUMENT NOs. (Any other numbers which may be assigned this document either by the originator or by the sponsor.)

11. DOCUMENT AVAILABILITY (any limitations on further dissemination of the document, other than those imposed by security classification)

(X) Unlimited distribution
( ) Defence departments and defence contractors; further distribution only as approved
( ) Defence departments and Canadian defence contractors; further distribution only as approved
( ) Government departments and agencies; further distribution only as approved
( ) Defence departments; further distribution only as approved
( ) Other (please specify):

12. DOCUMENT ANNOUNCEMENT (any limitation to the bibliographic announcement of this document. This will normally correspond to the Document Availability (11). However, where further distribution (beyond the audience specified in (11) is possible, a wider announcement audience may be selected).

13. ABSTRACT (a brief and factual summary of the document. It may also appear elsewhere in the body of the document itself. It is highly desirable that the abstract of classified documents be unclassified. Each paragraph of the abstract shall begin with an indication of the security classification of the information in the paragraph (unless the document itself is unclassified) represented as (S), (C), (R), or (U). It is not necessary to include here abstracts in both official languages unless the text is bilingual).

Magnetic shape memory alloys based on the Heusler alloy Ni_2MnGa have been investigated experimentally and the magnetic interactions have been modeled on the basis of the indirect exchange coupling of localized magnetic moments. A variety of techniques including x-ray diffraction, differential scanning calorimetry, thermogravimetric analysis, magnetization and Mössbauer effect spectroscopy have been utilized to measure the structural, thermal and magnetic properties of these alloys. Analysis of these results suggests that alloys containing a few at% Fe may be the most suitable for further exploration as commercially viable magnetic shape memory alloys. Theoretical investigations have shown that the indirect exchange coupling of magnetic moments associated with Mn ions on the Mn sites with other Mn-site Mn moments is ferromagnetic. This is also the case for Ni site moments associated with Ni ions. The coupling between Mn-site Mn moments and Mn ions located on Ni or Ga sites is antiferromagnetic. These observations explain the composition dependence of the saturation magnetization and the Curie temperature in off-stoichiometric Ni_2MnGa alloys.

14. KEYWORDS, DESCRIPTORS or IDENTIFIERS (technically meaningful terms or short phrases that characterize a document and could be helpful in cataloguing the document. They should be selected so that no security classification is required. Identifiers, such as equipment model designation, trade name, military project code name, geographic location may also be included. If possible keywords should be selected from a published thesaurus. e.g. Thesaurus of Engineering and Scientific Terms (TEST) and that thesaurus-identified. If it not possible to select indexing terms which are Unclassified, the classification of each should be indicated as with the title).

Magnetic shape memory alloys, Ni-Mn-Ga-X, magnetic interactions, models, exchange coupling

This page intentionally left blank.

Defence R&D Canada

Canada's leader in defence
and National Security
Science and Technology

R & D pour la défense Canada

Chef de file au Canada en matière
de science et de technologie pour
la défense et la sécurité nationale

www.drdc-rddc.gc.ca